Journal of Structural Geology 33 (2011) 78–91

Contents lists available at ScienceDirect

Journal of Structural Geology

journal homepage: www.elsevier.com/locate/jsg

# Mechanical analysis of fault slip data: Implications for paleostress analysis

J.O. Kaven [a,*], F. Maerten [b], D.D. Pollard [c]

[a] Now at U.S.G.S. Menlo Park, Menlo Park, CA 94025, USA
[b] IGEOSS, A Schlumberger Company, 34790 Grabels, France
[c] Department of Geological and Environmental Sciences, Stanford University, Stanford, CA 94305, USA

ARTICLE INFO

*Article history:*
Received 21 September 2010
Received in revised form
12 November 2010
Accepted 6 December 2010
Available online 10 December 2010

*Keywords:*
Fault slip data
Paleostress
Stress inversion
Mechanical interaction

ABSTRACT

Stress inversions are a useful and popular tool for structural geologist and seismologist alike. These methods were first introduced by Wallace (1951) and Bott (1959) and subsequent studies continue to be based on their assumptions: the remote stress tensor is spatially uniform for the rock mass containing the faults and temporally constant over the history of faulting in that region, and the slip on each fault surface has the same direction and sense as the maximum shear stress resolved on that surface from the remote stress tensor. Furthermore, successful implementation requires that slip accumulates on faults of diverse orientation. Many studies employ these methods on isolated faults or on fault systems with limited ranges of orientations, which can lead to erroneous results. We propose a new method that incorporates the effects of mechanical interaction of the entire fault or fault system, and solves the complete mechanical problem rather than employing empirical relationships between slip and stress or strain (or strain rate). The method requires knowledge of the fault geometry and information on at least one slip vector component along portions of the known fault geometry. For example, if throw is known, the strike-slip component can be solved for. We test the method using a single synthetic fault with anisotropic roughness similar to that measured at fault outcrops. While the orientation of remote stress may be determined precisely, the lack of diverse fault orientations introduces a systematic error in the remote stress ratio. We further test the effect of diversity of fault orientations and find that Wallace–Bott type inversions do not perform as well for limited ranges of orientations when compared to the proposed method. Finally, we use published data from the 1999 Chi-Chi, Taiwan, earthquake, and find that the method using surface data only, and surface data with subsurface focal mechanisms, produce similar results. The resulting stress orientations are in good agreement with results from Wallace–Bott inversions. Furthermore, the slip distribution is in general agreement with kinematic slip inversions using coseismic surface deformation. Stress inversion methods using fault slip data can thus be improved upon, significantly in some cases, by solving a mechanical boundary value problem that takes into account the geometry of faults or fault systems. As a bonus, the solution provides the stress, strain, and displacement fields throughout the region and the slip distributions on the faults.



## 1. Introduction

Over the course of the 20th Century geologists sought to understand the origin and evolution of faults, and the tectonic history of faulted regions, by relating fault orientation and slip direction to the state of stress in Earth's crust (e.g. Anderson, 1942; Price, 1966; Voight, 1966; Mandl, 1988). This relationship may be elucidated through both forward and inverse problem solving. In typical forward problems the equations of motion are solved with a prescribed remote stress state as boundary conditions, yielding the local stress, strain, and displacement fields, and the slip distributions over the model faults (e.g. Hafner, 1951; Sanford, 1959; Couples, 1977; Bürgmann et al., 1994; Willemse et al., 1996; Maerten et al., 1999). Assumptions about the constitutive behavior, the magnitudes of the strains, and the relative magnitudes of dynamic and static forces (Malvern, 1969, Chapters. 6, 4, and 8, respectively) enable one to reduce the underlying conservation laws to the relevant equations of motion (Pollard and Fletcher, 2005, Chapter 7). While the correspondence of such models to faulting in Earth's crust depends upon the accuracy of the assumptions, each of which requires careful assessment, the efficacy of the methodology rests securely on the foundation of a complete mechanics (Fletcher and Pollard, 1990).

* Corresponding author.
*E-mail addresses:* okaven@usgs.gov (J.O. Kaven), fmaerten@igeoss.com (F. Maerten), dpollard@standard.edu (D.D. Pollard).

0191-8141/$ – see front matter © 2010 Elsevier Ltd. All rights reserved.
doi:10.1016/j.jsg.2010.12.004

In typical inverse problems the directions of the remote principal stresses and a ratio of their magnitudes are constrained by analyzing field data on fault orientations and slip directions as inferred from striations such as slickenlines on exposed fault surfaces (e.g. Carey and Brunier, 1974; Etchecopar et al., 1981; Angelier et al., 1982; Gephart and Forsyth, 1990; Angelier, 1984; Michael, 1987; Reches, 1987; Fry, 1999; Shan et al., 2004). The adoption of this methodology is facilitated by an instructive exposition and computer codes in the textbook by Ramsay and Lisle (2000) and by the availability of other computer codes (e.g. Huang, 1988; Hardcastle and Hills, 1991; Orife et al., 2002). The enthusiastic implementation of the methodology by the structural geology community is witnessed by global compilations of paleostress results from 250 sites for the World Stress Map Project (Reinecker et al., 2004) and from 2791 independently chosen sites (Lisle et al., 2006) for a Special Issue of the Journal of Structural Geology on "New Dynamics in Palaeostress Analysis" (Blenkinsop et al., 2006). The equations of motion are not invoked for this inverse problem, and perturbations of the local stress field by fault slip are ignored. In other words, the mechanical role played by the faults in the tectonic deformation is not included explicitly in the analysis. Instead, two basic assumptions are made:

1. The stress field is spatially homogeneous and temporally constant; and
2. The direction of slip and the direction of the maximum shear stress resolved on each would-be fault plane are coincident.

These assumptions enable the inversion, which uses Cauchy's Formula (Fung, 1977, p. 62) to relate the tangential tractions (maximum shear stresses) on planes with the measured fault orientations to the principal stresses in the corresponding homogeneous stress field.

In a remarkably prescient paper, which to our knowledge is the earliest example of paleostress inversion, Anderson (1905) began, without comment or justification, by simply taking one principal stress direction as vertical at any point. This assumption was addressed explicitly 37 years later by Anderson (1942, p. 12 and Chapter VII). In his 1905 paper Anderson suggested that planes carrying the maximum tangential stress "will have much to do with determining the directions of faults in the rock". He understood that there are two orientations of such planes at any point; that these planes intersect in the direction of the intermediate principal stress; and that they make equal angles of 45° to the greatest principal compressive stress. He extended these relationships for stress at a point to rock volumes encompassing faults and conceived two conjugate sets of would-be faults corresponding to a single state of homogeneous stress. In calculating the resolved tangential stress on the conjugate planes Anderson used a variant of the Cauchy Tetrahedron (Malvern, 1969, p. 73) with one face corresponding to a would-be fault and made an interesting analogy: "This prism we suppose to exist in the rock, somewhat as the statue exists beforehand in the block of marble…" Apparently Anderson understood that slip on an actual fault would perturb the stress from its assumed homogeneous state. We appeal to his analogy of the would-be statue residing in the block of marble and refer to the entire class of inverse problems based on a homogeneous stress state as *faultless paleostress analysis*.

The next stage in the development of faultless paleostress analysis was introduced in the middle of the last century when Wallace (1951) analyzed the maximum shear stress (tangential traction) on planes of arbitrary orientation for a homogeneous stress state using Cauchy's Formula (e.g. Jaeger et al., 2007, p. 31). He illustrated the magnitude and orientation of this shear stress on stereonets and Mohr diagrams. Appealing to laboratory results and Mohr's theory (Nádai, 1931, p. 61), Wallace proposed that "faults will tend to concentrate at orientations tangent to a cone, with apex angle less than 90° (45° radius), which has the axis of greatest compressive stress as its axis…" and that "Orientation of net slip on faults can be correlated almost directly with orientation of maximum shearing stress…". In summary, he suggested that "If a complete picture of fault-plane orientations and net-slip orientations on several faults is available, it should be possible to determine with some degree of certainty the orientation and nature of the stress system producing the faults."

Taking a somewhat different approach conceptually, Bott (1959) contemplated the likely presence of strength inhomogeneity in the form of older faults, joints, and cleavage. Apparently supposing that whatever perturbation in the stress field due to the formation of these structures had relaxed, he suggested "These planes would remain unnoticed until the shearing stress within them should exceed the strength…". Furthermore, Bott suggested "…fracture would occur within the preferred plane in which the strength was first exceeded, and the direction of the initial slip would be defined by the direction of the greatest shearing stress within the plane". Bott then preceded, as did Wallace (1951) to employ Cauchy's Formula (e.g. Jaeger et al., 2007, p. 31) to derive the equation relating the shear traction, $\tau$, to the principal stress magnitudes ($\sigma_1 \geq \sigma_2 \geq \sigma_3$):

$$\tau^2 = \sigma_1^2 n_1^2 + \sigma_2^2 n_2^2 \sigma_3^2 n_3^2 - \left(\sigma_1^2 n_1^2 + \sigma_2^2 n_2^2 \sigma_3^2 n_3^2\right)^2 \\ (\sigma_1 - \sigma_2)^2 n_1^2 n_2^2 + (\sigma_2 - \sigma_3)^2 n_2^2 n_3^2 + (\sigma_3 - \sigma_1)^2 n_3^2 n_1^2 \quad (1)$$

Here the principal stress directions are coincident with the coordinate axes and ($n_1$, $n_2$, $n_3$) are the components of the unit normal to the plane bearing the shear traction. Bott concludes that oblique slip faults may occur in any orientation for a given orientation of the principal stress axes if planes of suitable weakness lie in that orientation. In some of the modern literature cited below the coincidence of the tangential traction (direction of maximum resolved shear stress) and the slip direction is referred to as the 'Wallace–Bott' hypothesis.

A considerable effort has been made to distinguish and separate field measurements of slip directions attributable to stress states that vary in space or time, so-called heterogeneous data sets (e.g. Armijo et al., 1982; Angelier, 1984; Huang, 1988; Hardcastle and Hills, 1991; Nemcok and Lisle, 1995; Yamaji, 2000; Shan et al., 2003; Liesa and Lisle, 2004; Shan and Fry, 2005). At the same time methods have been devised for error estimation of the paleostress inversion (e.g. Angelier, 1984; Choi, 1996; Orife and Lisle, 2003; Shan et al., 2006; Sato and Yamaji, 2006), for example by comparing the misfit between the maximum shear stress directions (presumed slip directions) resolved from the preferred stress state and the measured slip directions on the respective faults. These are valuable procedures for the analysis, but they remain rooted in the two basic assumptions and therefore, while testing self-consistency and goodness of fit, they do not provide independent tests of the methodology. Shan et al. (2006) have pointed out several reasons that the basic assumptions would be violated, leading "to dispersion in the parameter space of measured fault/slip data, or even possibly the presence of superficially heterogeneous fault/slip data. For the latter, we have meaningless data groups and false estimated stresses through conventional inversion methods. This is indeed the Achilles' heel of stress inversion."

Two related topics must be acknowledged, because they have developed in parallel with, and sometimes intertwined with geological paleostress analysis. Seismological data are used to identify the quadrants that contain the so-called P and T axes for a given earthquake focal mechanism (e.g. McKenzie, 1969; Whitcomb et al.,

1974; Aki and Richards, 2002). Because the fault plane generally is not available to the seismologist, they face the additional ambiguity of two orthogonal would-be fault orientations that stem from the representation of seismic sources as double-couple force systems (Lay and Wallace, 1995; Vasseur et al., 1983; Michael, 1987; Gephart, 1990). Some researchers associate P and T with the axes of greatest shortening and greatest extension, that is principal strains or strain rates (Marrett and Allmendinger, 1990; Twiss et al., 1993; Twiss and Unruh, 1998), while others associate P and T with the axes of greatest and least compression, that is principal stresses (Angelier and Mechler, 1977; Gephart and Forsyth, 1990; Julien and Cornet, 1980; Jones, 1988; Michael, 1987; Ramsay and Lisle, 2000) for the fault in question. Whether the interpretation leads to principal strains, strain rates, or stresses, the reduction of what must be a heterogeneous field of these quantities around an active fault to a homogeneous representation (Brune, 1968; Kostrov, 1968; Molnar, 1983; Jackson and McKenzie, 1988) draws into question the first basic assumption stated above. We do not concern ourselves further with the seismological investigation of P and T, except in so far as the evaluation of this assumption might reflect upon it.

The second related topic is the interpretation of fault data by geologists in a kinematic context. That is, the orientations of faults and the slip directions inferred from striations upon them are associated with the directions of a homogeneous field of principal strains or strain rates and a ratio of their magnitudes (Reches, 1978, 1987; Aydin and Reches, 1982; Gauthier and Angelier, 1985; Wojtal, 1989; Twiss et al., 1991; Twiss and Unruh, 1998). Cladouhos and Allmendinger (1993) refer to "the strain due to a population of faults within a region" as the fault strain and investigate this homogeneous quantity for cases where the infinitesimal strain approximation used by those mentioned above is inappropriate (see also Gapais et al., 2000). Again, we do not concern ourselves further with the kinematic interpretation of fault slip inversions, except in so far as the evaluation of the homogeneous assumption might reflect upon it. Because the models we employ use an isotropic and linear elastic constitutive law, the principal stress and strain directions at any point are identical and the respective components are proportional. The method of inversion proposed here, whether for remote principal stresses or strains, applies the principles of continuum mechanics to a medium with explicit surfaces of discontinuity in the displacement field, which are the model faults.

In an extensive review of fault slip inversion methodology Twiss and Unruh (1998) evaluate the relative merits of stress and kinematic interpretations, emphasizing that the kinematic quantity of interest should be the rate of deformation rather than the strain or strain rate, and adding an additional unknown, the relative vorticity, to the inversion problem in order to account for local block rotations (Twiss et al., 1991). They distinguish the local scale of a single fault or earthquake rupture from the larger 'global' scale and assert: "From a global volume we need a sufficiently large set of fault slip data in order to find an inverse solution for the homogeneous principal deformation rates or the homogeneous principal stresses". As part of our evaluation of the second basic assumption we identify conditions under which such a global volume exists, and within which fault slip is dependent upon both the global state of stress and the mechanical interaction of the model faults. For the isotropic elastic solutions we employ, the relative vorticity is identically zero.

One purpose of this paper is to provide new evaluations of the basic assumptions of paleostress analysis. These assumptions have received some attention as the inversion method was put into practice (Carey-Gailhardis and Mercier, 1987; Dupin et al., 1993; Pollard et al., 1993; Orife and Lisle, 2003). In some studies independent data sets from seismology (earthquake focal mechanisms) or geodesy (displacements from GPS surveys) have been compared to fault slip directions (Roberts and Ganas, 2000; Kao and Angelier, 2001; Blenkinsop, 2006). A direct evaluation of the assumptions would require an independent measure of the tangential traction vector (maximum shear stress) acting on a fault surface during slip, so the direction of this vector could be compared to the slip direction. A direct evaluation also would require in-situ stress measurements at some distance from the active faults to establish the homogeneity of the remote stress field (e.g. Zoback et al., 1987; Zoback, 1992). Although technology exists today to infer the stress state from such measurements in active tectonic regions (Amadei and Stephansson, 1997), they are not possible for ancient faults. Instead, we evaluate the assumptions using a methodology similar to that employed in forward modeling that invokes the equations of motion and explicitly includes the faults and their associated fields of stress and deformation (Pollard et al., 1993; Maerten, 2000; Maerten et al., 2005). A second purpose of this paper is to draw attention to a new form of paleostress inversion using a complete mechanics and to encourage its use. The computer code used here is available from IGEOSS (http://www.igeoss.com/igeoss/) at a nominal cost for non-commercial research.

## 2. Accounting for a complete mechanics

The displacement discontinuity resulting from remotely applied stresses acting on fracture surfaces are governed by principles of continuum mechanics, dominantly those of linearly elastic theory that were first introduced by Inglis (1913), and Griffith (1921, 1925), and later developed by Irwin (1957) and Williams (1987) and many others, becoming a mature discipline (Lawn and Wilshaw, 1993; Anderson, 1995) by the end of the 20th century. The concepts of fracture mechanics have been used to explain a variety of rock fracture phenomena including aspects of faulting (see numerous examples in Atkinson, 1987). From these we understand that slip on a particular segment of a fault is determined not only by the remote stress or strain tensor, but also includes the effects of material properties of the surroundings (Lamé constants), and the fault surfaces (friction) or fault zone (strength), the orientation and geometry of the fault tipline and surfaces, and the effects of all other proximal segments of the fault or fault system. Both analytical (e.g. Rudnicki, 1980; Rice, 1980; Pollard and Segall, 1987; Bürgmann et al., 1994; Martel and Shacat, 2006) and numerical (e.g. Segall and Pollard, 1980; Willemse, 1997; Maerten et al., 2005) models have helped to elucidate these relationships. The problem at hand (multiple three-dimensional faults that interact mechanically with one another) requires the elastic boundary value problem to be solved numerically.

Boundary element methods (Crouch and Starfield, 1983), such as the displacement discontinuity method employed in the numerical code Poly3D (Thomas, 1993; Maerten et al., 2005) permit one to solve the elastic problem as a system of algebraic equations that relate the tractions on a triangular element of the fault surface to the displacement discontinuity on that element and all other elements that make up the fault or faults (Fig. 1). The system of linear equations has the following general form:

$$\begin{aligned}
\sum_{f=1}^{N} A_{ss}^{ef} D_s^f + \sum_{f=1}^{N} A_{sd}^{ef} D_d^f + \sum_{f=1}^{N} A_{sn}^{ef} D_n^f + \tau_s^e &= 0 \\
\sum_{f=1}^{N} A_{ds}^{ef} D_s^f + \sum_{f=1}^{N} A_{dd}^{ef} D_d^f + \sum_{f=1}^{N} A_{dn}^{ef} D_n^f + \tau_d^e &= 0 \\
\sum_{f=1}^{N} A_{ns}^{ef} D_s^f + \sum_{f=1}^{N} A_{nd}^{ef} D_d^f + \sum_{f=1}^{N} A_{nn}^{ef} D_n^f + \tau_n^e &= 0
\end{aligned} \qquad (2)$$

where $e, f = 1,\ldots,N$ and $N$ is the number of fault elements, $\tau_n$, $\tau_s$, $\tau_d$ are the normal, strike-parallel, and dip-parallel traction components at

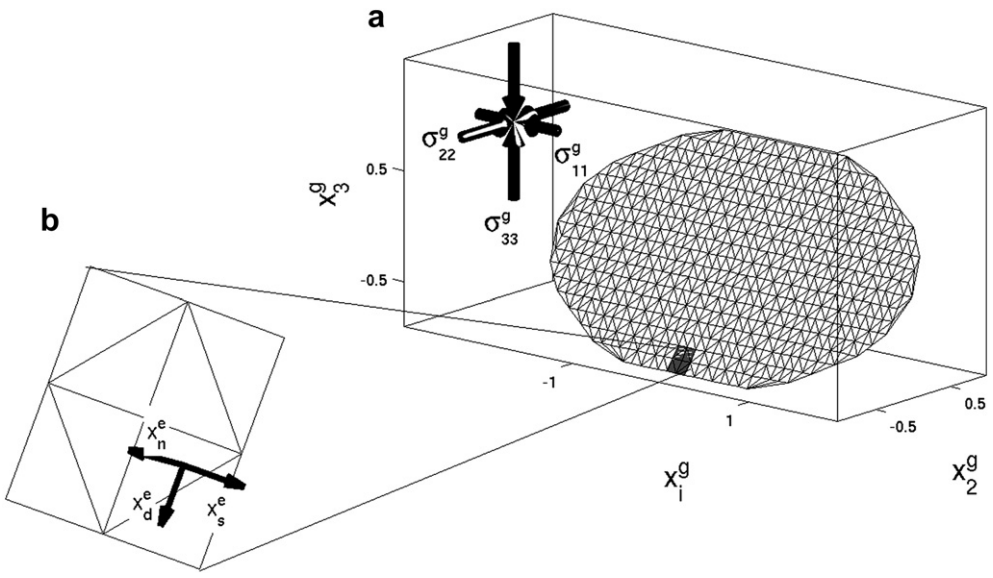


**Fig. 1.** Displacement discontinuity discretization, global (a) and local (b) reference systems and orientations of remote stresses.

the element center, respectively, and $D_n$, $D_s$, and $D_d$ are the uniform normal, strike-parallel and dip-parallel displacement discontinuity components between the two surface of the element, respectively (Fig. 1). The influence coefficient matrices $A_{kl}$ ($k,l = n,d,s$) relating the corresponding displacement discontinuity to the tractions follow from the analytical solution for the angular dislocation (Yoffe, 1960) in the half-space (Comninou and Dunders, 1975) as extended to the polygonal surface of displacement discontinuities by Jeyakumaran et al. (1992). The element local quantities are expressed in terms of the local coordinate axes (Fig. 1) and require transformations into the global coordinate axes system, which can be done in the computation of the influence coefficients directly. In general, the problem at hand may be one with mixed boundary conditions (e.g. normal displacement discontinuity components and both strike- and dip-parallel tractions), so equation (2) requires restructuring to properly constrain the solution. In the remainder of this paper, $A^{ef}$ denotes the traction influence matrix at a field element $e$ due to a source element $f$ with slip vector $D_f$. It is implied that these quantities account for all three vector components at a particular element. The general "forward" problem of sliding on interacting faults, i.e. when either slip, tractions, or a combination of both are known along the entire fault and the remote stresses are known, is solved using equation (2).

The unknown displacement discontinuity vector at element $e$ can be computed with an iterative scheme using a block Gauss-Seidel like definition (Maerten et al., 2010):

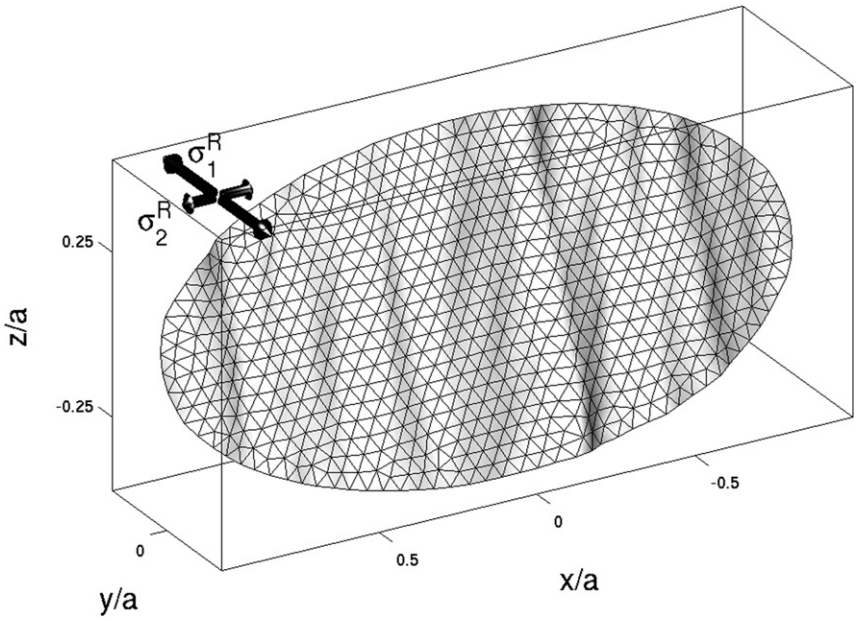


**Fig. 2.** Anisotropically rough synthetic fault surface used in forward models to generate slip given the applied remote stresses (arrows). Note that only horizontal stresses are applied. Lighting used to accentuate fault roughness.

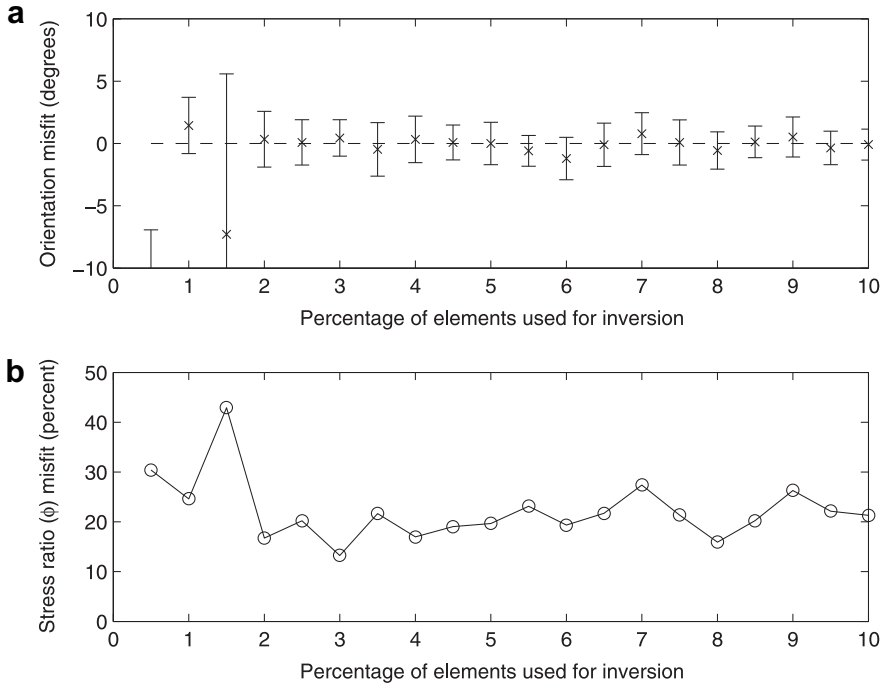


**Fig. 3.** Validation of results for varied percentage of elements used on a rough fault. 1% equals 14 elements used. a) Misfit in degrees of orientation of horizontal principal stress from inversion. b) % error in principal stress ratio, $\phi$, from inversion results.

$$\tau_e = -A_{ee}D_e - \sum_{f \neq e} A_{ef}D_f \tag{3}$$

which gives:

$$D_e = -A_{ee}^{-1}\left\{\tau_e^0 + \sum_{f \neq e} A_{ef}D_f\right\} \tag{4}$$

In general, it is assumed that some components of displacement discontinuity $D_e$ for element $e$ are unknown. In paleostress analyses, $D_e$ is known at outcrops but nowhere else along the fault. The matrix $A_{ee}^{-1}$ relates the known traction of element $e$ to its relative displacement. $\tau_e^0$ represents the initial boundary traction for an element $e$, and is determined from the resolved far field stress $\sigma^R$ onto this element in the local coordinate system using Cauchy's formula with appropriate rotation:

$$\tau_e = \omega_e \sigma^R n_e \tag{5}$$

where $n_e$ is the element normal unit vector. The rotation matrix $\omega_e$ relates the remote stresses to the element local along-strike, along-dip, and normal traction components and is comprised of direction cosines.

Confining pressures in the crust tend to suppress opening of faults, so we enforce the condition that the normal relative displacement is zero. This condition is known to be violated near steps and bends in faults and near terminations of faults that are accompanied by splay cracks (Mutlu and Pollard, 2008). Using the Andersonian stress state (Anderson, 1942), that is a traction-free surface and negligible topography, the vertical stress, $\sigma_{33}^R$, is a principal stress (implying $\sigma_{13}^R = 0 = \sigma_{23}^R$), so:

$$\sigma^R = \begin{bmatrix} \sigma_{11}^R & \sigma_{12}^R & 0 \\ \sigma_{21}^R & \sigma_{22}^R & 0 \\ 0 & 0 & \sigma_{33}^R \end{bmatrix} \tag{6}$$

The validity of this stress state is corroborated by data from numerous locations and appears typical of crustal stresses (Lisle et al., 2006). By orienting the global coordinate axes so the third normal stress component is vertical we can modify the definition of the normal far field stress so the diagonal components of this tensor also depend on the magnitude of the vertical stress. Furthermore, since the addition of an isotropic stress does not change the resolved tractions on faults, equation (6) can be simplified to:

$$\sigma^R = \begin{bmatrix} \sigma_{11}^R - \sigma_{33}^R & \sigma_{12}^R & 0 \\ \sigma_{12}^R & \sigma_{22}^R - \sigma_{33}^R & 0 \\ 0 & 0 & 0 \end{bmatrix} \tag{7}$$

which then permits one to rewrite the sought after stress tensor components as:

$$\tilde{\sigma}^R = \begin{bmatrix} \tilde{\sigma}_{11}^R & \sigma_{12}^R \\ \sigma_{12}^R & \tilde{\sigma}_{22}^R \end{bmatrix} \tag{8}$$

where the tilde signifies the difference between horizontal normal stress components and the vertical normal stress. Anderson's standard state of stress thus provides the basis for the above assumptions, i.e. the horizontal perturbations to lithostatic stress with one principal stress vertical.

Now, consider a model comprised of $N$ triangular elements (Fig. 1) with traction boundary conditions for the strike and dip components and a displacement discontinuity condition for the normal component with magnitude zero. For a given element $e$, two equations need to be solved:

$$\begin{aligned} -\tau_{e,s}^0 &= \left(\sum_f A_{ef}D_f\right)_s \\ -\tau_{e,d}^0 &= \left(\sum_f A_{ef}D_f\right)_d \end{aligned} \tag{9}$$

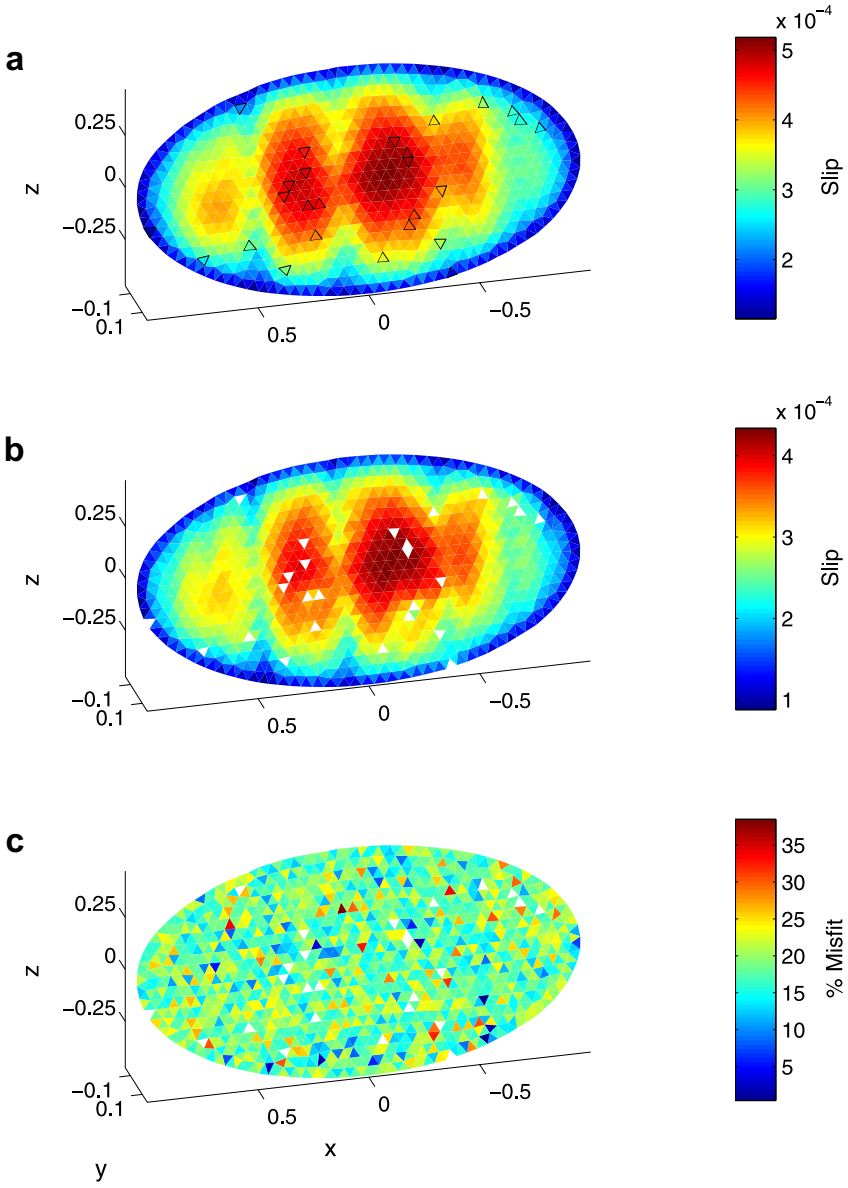


**Fig. 4.** a) Slip magnitude on heuristic fault model from the forward model. The approximately self-affine surface roughness is larger in the direction parallel to strike. Random triangles used in inversions or outlined in black. b) Inverted slip distribution using the select elements. c) % misfit of slip distribution between the forward model and the inversion result.

where $\tau^0_{e,s}$, $\tau^0_{e,d}$ and some of the displacement discontinuity vectors $D$ are unknown. Subscript commas do not indicate differentiation.

Combining equations (5) and (6), and recognizing that the remote stress tensor consists of four independent components, we get:

$$-{}^{\omega}{}_{e}\begin{Bmatrix}\sigma^R_{11}\\ \sigma^R_{12}\\ \sigma^R_{22}\\ \sigma^R_{33}\end{Bmatrix} = \begin{Bmatrix}\left(\sum_f A_{ef}D_f\right)_s\\ \left(\sum_f A_{ef}D_f\right)_d\end{Bmatrix} \tag{10}$$

$$-\tilde{\omega}_e\begin{Bmatrix}\tilde{\sigma}^R_{11}\\ \sigma^R_{12}\\ \tilde{\sigma}^R_{22}\end{Bmatrix} = \begin{Bmatrix}\left(\sum_f A_{ef}D_f\right)_s - \omega_{e,13}\sigma^R_{33}\\ \left(\sum_f A_{ef}D_f\right)_d - \omega_{e,23}\sigma^R_{33}\end{Bmatrix} \tag{11}$$

where $\omega_{e,ij}$ are the direction cosines relating the element local traction components to the remote stresses. For a given known or estimated value of $\sigma^R_{33}$ equation (11) in simplified form (using equation (9)) becomes:

$$-\tilde{\omega}_e\begin{Bmatrix}\tilde{\sigma}^R_{11}\\ \sigma^R_{12}\\ \tilde{\sigma}^R_{22}\end{Bmatrix} = \begin{Bmatrix}\tilde{\tau}^0_{e,s}\\ \tilde{\tau}^0_{e,d}\end{Bmatrix} \tag{12}$$

where $\tilde{\tau}^0_{e,s} = \tau^0_{e,s} - \omega_{e,13}\sigma^R_{33}$ and $\tilde{\tau}^0_{e,s} = \tau^0_{e,s} - \omega_{e,23}\sigma^R_{33}$.

Using a Least Squares formulation (Aster et al., 2005, p. 16) for all elements, we find:

$$\begin{Bmatrix}\tilde{\sigma}^R_{11}\\ \sigma^R_{12}\\ \tilde{\sigma}^R_{22}\end{Bmatrix} = \left(\tilde{\omega}^{\tau}\tilde{\omega}\right)^{-1}\tilde{\omega}^{t}\begin{Bmatrix}\tilde{\tau}^0_{e,s}\\ \tilde{\tau}^0_{e,d}\end{Bmatrix} \tag{13}$$

We solve for the best-fitting unknown remote stress and resultant slip distribution on portions of the fault or fault system where no slip data are available.

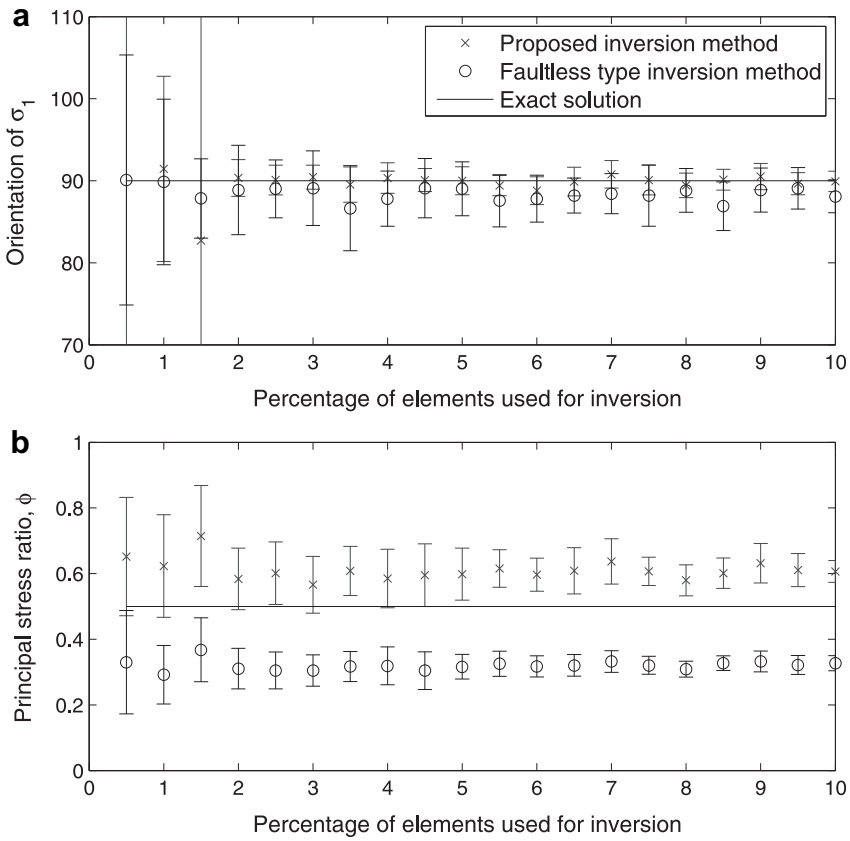


**Fig. 5.** a) Orientation of horizontal principal stress for varied percentage of elements used in mechanics-based stress inversion and faultless inversions. 1% equals 14 elements used. Error bars indicate variance within 20 model runs for each constellation of elements. Principal stress orientation imposed in forward models is 90°. b) Principal stress ratio, $\phi$ ($\phi = 0.5$ in forward models), from mechanics-based and faultless inversions for varying percentage of elements used.

Note that equation (13) solves for the unknown $\tilde{\sigma}^R$ using the computed traction vector, while equation (4) solves for the unknown slip vectors using the resolved traction vector $\tilde{\tau}_e^0$. Therefore, the solution algorithm has two steps: 1) use the initial remote stress tensor $\tilde{\sigma}^R$, resolve it onto the fault elements that have no relative displacement data, and solve for the unknown relative displacements; 2) use the computed and known relative displacements to solve for $\tilde{\sigma}^R$. We choose an iterative solver that cycles between steps 1) and 2) until convergence. The determination of the relative displacement vectors for the elements is constrained by the resolved far field stress, which makes this method different from a linear slip inversion (Maerten et al., 2005). This process is outlined in Algorithm 1.

**Algorithm 1**. Paleostress iterative solver.

**Data** : Known slip vectors: $D_k$

**Model**: Unknown slip vector, $D_u$, and remote stress, $\tilde{\sigma}^R$

initialization: Set starting guess for $D_u$ and $\tilde{\sigma}^R$

**while** *not converged* **do**

→ $\mathbf{S_1}$: Solve for the $D_u$ for each element $e$ using the resolved $\tilde{\sigma}^R$ and $D_k$

→ $\mathbf{S_2}$: Solve the unknown $\tilde{\sigma}^R$ using $D_u$ and $D_k$

→ **Post processing**: Resolve $\tilde{\sigma}^R$ onto each element $e$ and set as initial boundary conditions

**end**

Once the algorithm has converged, the full stress tensor can be obtained by adding the isotropic normal stress to the diagonal components (equations (6) and (7)). Then the Cartesian stress components $\sigma_{11}^R$, $\sigma_{12}^R$, $\sigma_{22}^R$ are used to retrieve the orientation of the horizontal principal axes of the stress tensor and their magnitudes. Numerical verification, convergence, and speed considerations are presented in detail in Maerten et al. (2010).

## 3. Test results for stress inversion

We test the proposed algorithm (Algorithm 1) by comparing results of the inversion to those from a typical faultless stress inversion. Our general strategy for these tests is to solve the forward problem, i.e. subjecting a fault of known geometry to a known remote stress tensor and solving for the slip on the fault. We then use randomly picked portions of the faults (fault elements) and their slip vectors to invert for the stress tensor using the proposed method and faultless paleostress methods. We use single faults with non-planar surfaces, solve the forward problem to determine the slip on every element, randomly select varying fractions of the elements for inversion, and evaluate the errors and variances of the results. Then we use the same randomly selected slip data in a faultless inversion, and compare the results. We employ the same strategy to test a multi-fault system with varying orientations of the individual faults. Finally, we use field data from the 1999 Chi-Chi earthquake along the Chelungpu fault in Taiwan and contrast the results from these methods.

### 3.1. Heuristic example: single fault inversions

We test synthetic models of isolated faults with elliptical fault tiplines, but non-planar fault surface topography. The resultant limited variety of fault orientations makes this test an end-member

case. We include the single fault test here to highlight the shortcomings of both faultless and a complete mechanics stress inversions when fault orientations vary little. We evaluate the error in our inversion technique using the magnitudes and orientations of the remote stresses applied in the forward models. The fault surfaces have anisotropic, approximately fractal roughness with the slip-parallel direction being smoother than the slip-perpendicular direction (Fig. 2), and the roughnesses correspond to values from the faults measured by Sagy et al. (2007), which are normal faults of the Klamath Graben system with ≈100 m offset. We choose a non-planar fault geometry because the available data (e.g. Power et al., 1987; Sagy et al., 2007) indicate faults have significant non-planarity or roughness.

We estimate error and variance bounds for the mechanics-based method for the idealized fault (Fig. 3) by varying the percentages of elements used. For each percentage of elements tested we first choose fractal, anisotropically rough faults and solve the problem in a forward sense for the slip magnitudes and directions on every element given a remote stress that acts to induce dip-slip on the fault. The reduced horizontal remote

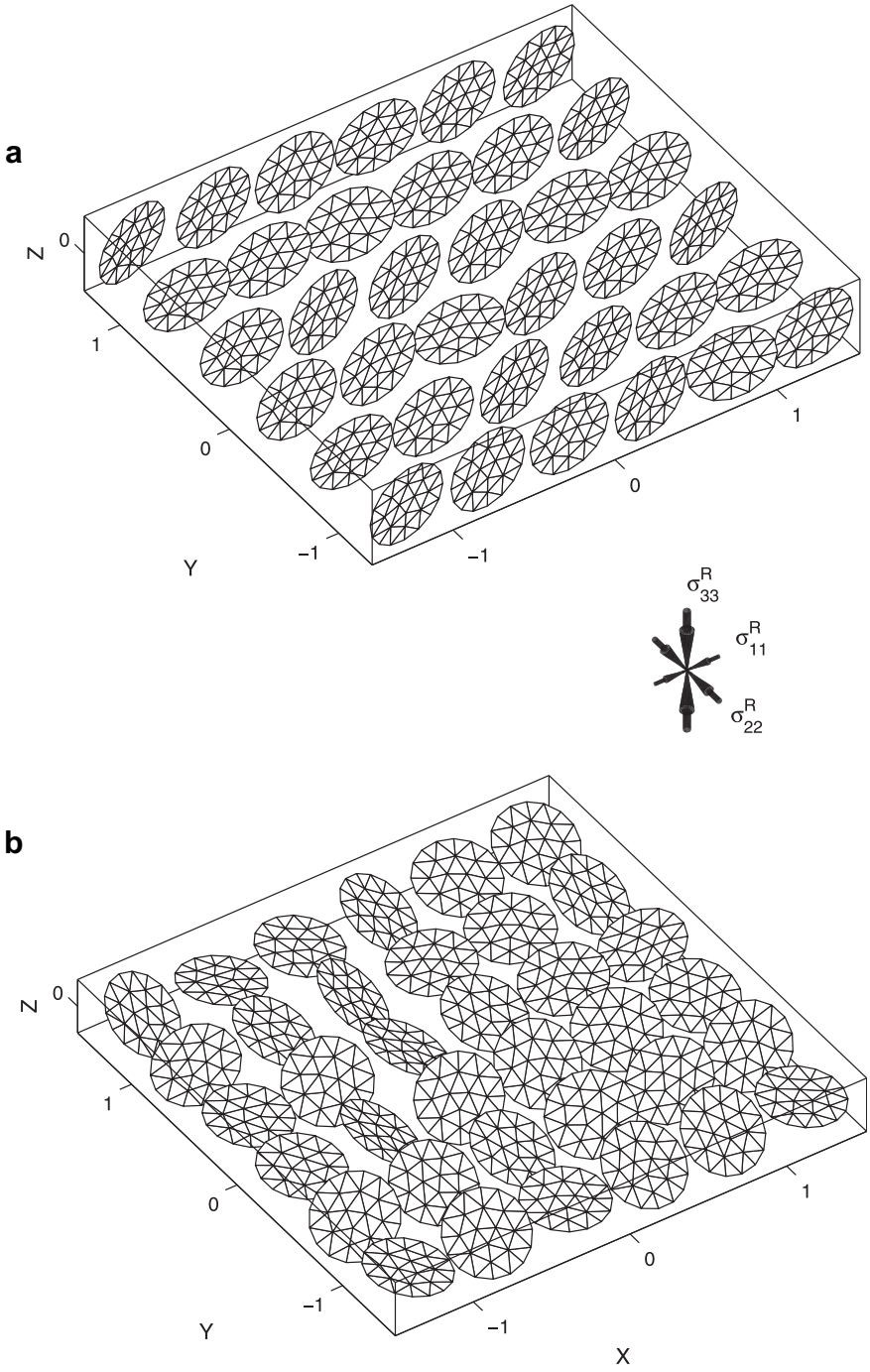


**Fig. 6.** Setup of heuristic models using various orientations: 36 faults are centered on fixed positions and allowed to randomly vary in strike and dip by (top) 20° and 5°, respectively, and (bottom) 160° and 80°, respectively. The remotely applied principal stresses are equivalent for all setups and indicated by the pairs of arrows. Boundary conditions on the faults are zero opening/closing and complete shear stress drop.

stresses are $\tilde{\sigma}_1^R = \tilde{\sigma}_{11}^R = 5$ MPa (recall $\tilde{\sigma}_{11}^R = \sigma_{11}^R - \sigma_{33}^R$), normal to fault strike, $\tilde{\sigma}_2^R = \tilde{\sigma}_{22}^R = 2.5$ MPa parallel to fault strike. The elastic properties of the isotropic and homogeneous medium are Young's modulus $E = 5$ GPa and Poisson's ratio $\nu = 0.25$. The boundary conditions on the fault prohibit interpenetration and result in a complete shear stress drop on all of the 1349 elements. From the resultant slip distribution we randomly select 20 constellations of elements and invert for the remote stress state using each. Then, we evaluate the mean stress orientation and the standard deviation.

The prescribed principal horizontal stress orientations are approximated very well by the proposed inversion method (Fig. 3a). The greatest mean angular misfit is 23° for 0.5% (7) elements used. Variances (standard deviations) in the inversion results are large (>16°and >12°) for the two cases with largest angular misfits likely due to switching of the horizontal principal stress orientations. This result clearly is anomalous, but indicates the possibility of significant and unanticipated error for inversions with less than about 30 measurements of slip. Misfits of principal stress ratios generally decrease with percentage of elements used up to 2% (28), but remain greater than 20% for all tests up to 10% (135) elements used (Fig. 3b). This apparent systematic error in the stress is attributed to the modest range of orientations of the synthetic fault surface. The spherical variance of the normals to all elements is $S_s^2 \geq 0.99$. While the chosen roughness is similar to that measured on fault surfaces at the outcrop scale, the range of orientations for the surface (or zone) of a particular fault at the kilometer scale can be much greater (e.g. Carena and Suppe, 2002; van Gent et al., 2010). As we show below, a greater range of orientations improves the quality of the inversion.

The mechanics-based methods permit one to solve for the slip distribution at every element on the fault (Fig. 4). The distribution of slip is approximately elliptical as expected for an isolated planar fault with elliptical tipline (Willemse et al., 1996, 1997). Deviations from an elliptical distribution are due to the non-planar fault surface, yielding heterogeneous resolved tractions, which, in turn, perturb the slip. From the known slip distribution of the forward model we randomly select elements used for an inversion (Fig. 4b) and calculate the misfits (Fig. 4c).

We compare the remote horizontal stress magnitudes and orientations of the proposed inversion technique to those from the method proposed by Michael (1987), which solves the faultless inversion problem. We expect that other codes and methods based on the same assumptions used to solve the faultless inversion problem will compare similarly, and choose this one merely as an example. We establish error and variance bounds for the idealized fault (Fig. 2) by varying percentages of elements used for the inversion (Fig. 5). We use the same constellations of elements, their local orientations and the slip on them to solve for the remote stress orientations (see details above).

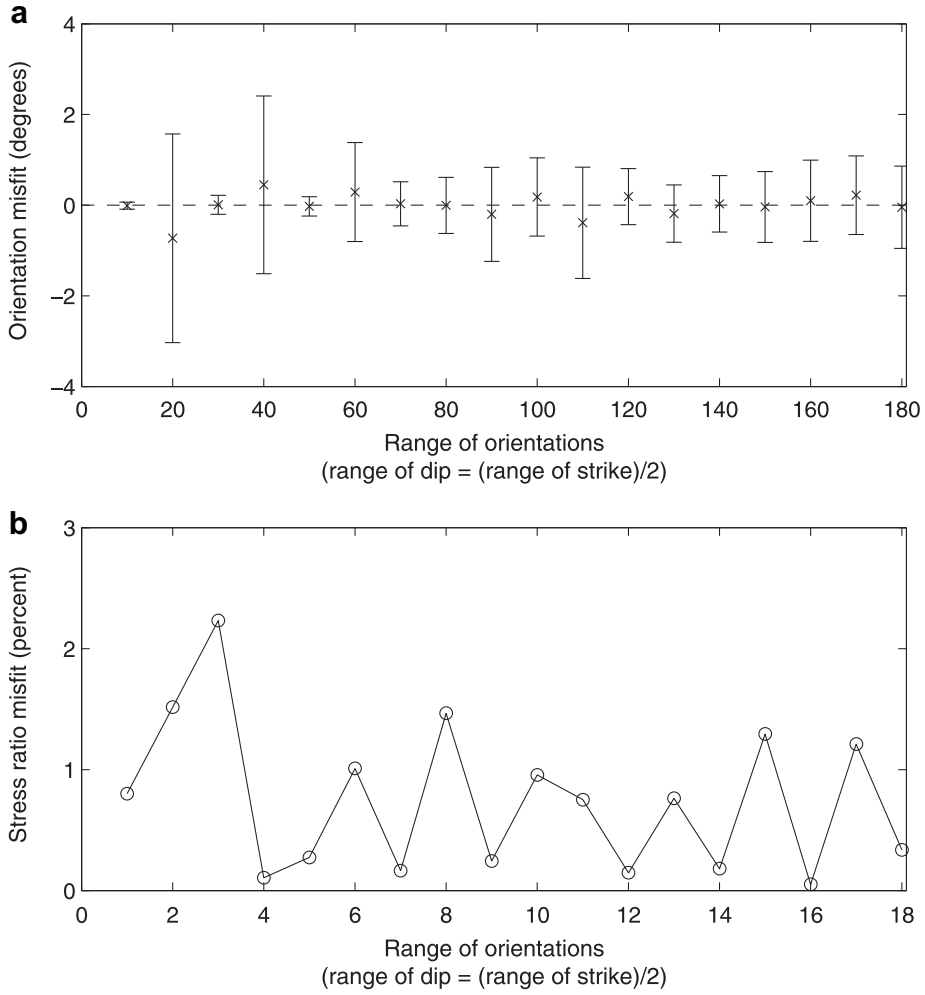


**Fig. 7.** Validation of results for various orientations within fault system, for setup see Fig. 6. a) Misfit in degrees of orientation of horizontal principal stress from inversion. b) % error in principal stress ratio, $\phi$, from inversion results.

Both methods do a good job of reproducing the mean stress orientation (normal to strike, 90°) imposed in the forward models (Fig. 5a). With 0.5% (14) elements or more, the mean orientations from the faultless stress inversion methods deviate by at most 4.5° and usually as little as 0.5° from the correct value. The method proposed here deviates by as much as 23° when 0.5% (7) of elements are used, but converges quickly on the correct orientation with more elements. The proposed method has greater variances than faultless inversion methods for models with few >1.5% (<21) elements used, but has reduced variance when more elements are used.

Neither method performs well in reproducing the principal stress ratio for the given setup (Fig. 5b). All estimates from the proposed method are off by 20% or more, and the faultless method is off by greater than 30%. Variances in principal stress ratio decrease for both methods with increased number of elements used, but there apparently is a systematic error for both. The difficulty in reproducing the stress ratio in both methods underscores the importance of varied fault orientations, which usually would not be sufficient if the data were restricted to one fault.

### 3.2. Heuristic example: fault system with diverse orientations

One of the commonly unenforced requirements of the faultless inversion is the necessity to include a variety of fault orientations within the fault system (Twiss and Unruh, 1998). Here we test the effects of diversity of fault orientations on both faultless and proposed stress inversion results by populating the fault system with non-intersecting planar circular faults at equal centroid spacing, but varying the individual orientations of the faults (Fig. 6). We choose planar circular faults to minimize the effects of roughness and tipline shape and to provide insight into the effects of fault system interaction and diverse orientations. We use a ratio of spacing over fault-radius of 5% (minimum) to avoid spurious numerical results, however, the model faults are mechanically interacting (Willemse et al., 1997). We follow the same strategy laid out in the preceding section of running forward models to produce the reference solution and slip on every element, some of which are selected randomly to constrain the inversions. We acknowledge that our model setup grossly underestimates the complications and does not represent all mechanisms present in a real fault system, but contend that the multiple fault scenario is an important one to test and contrast with results of the faultless inversion.

We center 36 circular faults on an evenly spaced grid (Fig. 6), allow a variety of strikes and dips for each fault in each forward model, select 5% of the elements for the combined stress and slip distribution inversion using 20 randomly selected constellations, and evaluate the mean errors and standard deviations for each setup. The range of strike orientations is permitted to vary in increments of 10°. Corresponding to the range in strike, we vary the dip of each fault in increments of 5°. The least range in orientations has strike varying from −5° to 5° and dips varying from 85° to 90°. The greatest range in orientations has strikes

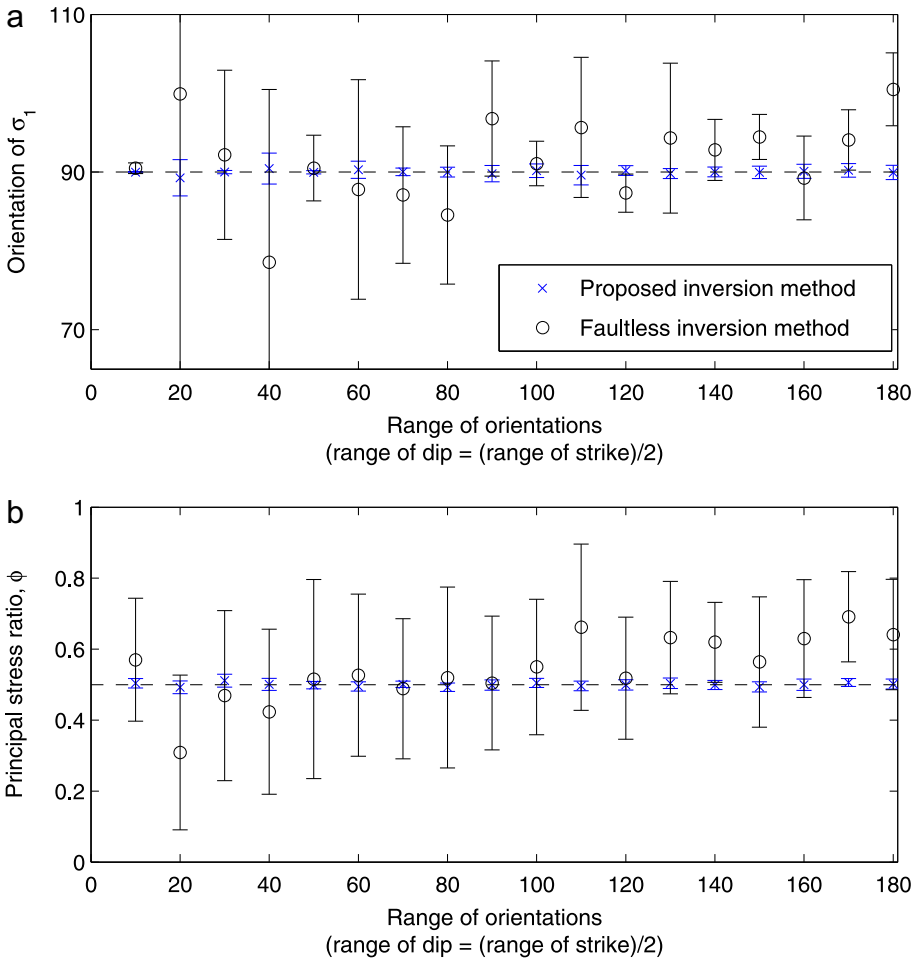


**Fig. 8.** a) Orientation of horizontal principal stress for varied ranges of fault orientations from mechanics-based stress inversion and faultless inversions. Error bars indicate variance within 20 model runs for each constellation of elements. b) Principal stress ratio, $\phi$, from mechanics-based and faultless inversions for varying orientations used.

varying from −90° to 90°, and dips varying from 0° to 90°. This gives a total of 18 cases for variations of strike and dip. The remote stresses are $\tilde{\sigma}_1^R = \sigma_{22}^R - \sigma_{33}^R = 5$ MPa, $\tilde{\sigma}_2^R = \sigma_{11}^R - \sigma_{33}^R = 2.5$ MPa. The boundary conditions on the fault prohibit opening or closing and result in a complete shear stress drop. The homogeneous, isotropic, and linearly elastic medium has Young's modulus $E = 5$ GPa and Poisson ratio $\nu = 0.25$.

The resulting horizontal principal stress orientations closely fit the applied stresses in the forward model (Fig. 7a): mean misfits are small (<0.5°) and standard deviations are all less than 2.5°. The stress ratio, $\phi = 1/2$, is reproduced well by the proposed inversion method, since the misfit is less than 2.5% for all fault models (Fig. 7b).

The sensitivity of the results to the range of fault orientations is compared for both inversion methods in Fig. 8. The proposed inversion technique produces results that are both very close to the imposed principal stress orientation and exhibit a small variation. The greatest mean error does not exceed 1° with standard deviations less than 0.5° for all ranges of orientations plotted. The faultless inversion technique (Michael, 1987) exhibits greater mean errors and greater standard deviations (Fig. 8). Mean errors are as great as 15° for a range of 20° in strike and 5° in dip. The principal stress ratio is in error by as much as 80%. However, both mean error and standard deviation are reduced as the diversity of orientations is increased. The proposed methodology provides a better reproduction of the forward models than the faultless methods: these results highlight the importance of mechanical interaction in fault systems and thus address fundamental limitations of the faultless methods.

### 3.3. Field example: 1999 Chi-Chi earthquake, Taiwan

Here we highlight the capabilities of the inversion method for a fault that has been studied extensively because it hosted the 1999 Chi-Chi earthquake. We focus in particular, on the paleostress inversions (e.g. Lee et al., 2003; Blenkinsop, 2006). The earthquake was a consequence of the ongoing collision of the Phillipean Sea and Eurasian plates; the fault ruptured along a surface trace of about 100 km and produced some of the largest surface slip ever recorded during a reverse faulting event (Lee et al., 2003). The fault trace itself is continuous except near the distal ends in the north and to a lesser extent in the south (Fig. 9). Along the fault trace 94 slip measurements have been reported (Lee et al., 2003) that have provided the basis for several studies of the stress orientations (e.g. Lee et al., 2003; Blenkinsop, 2006).

GPS surface displacements near the fault and throughout Taiwan have been used to kinematically invert for the coseismic slip on the fault (Johnson and Segall, 2004). Several studies have explored the focal mechanisms preceding, during, and after the main shock and provide a wealth of subsurface slip data, some of which occurred on the main shock rupture surface (Wu et al., 2008). Given the wealth of geologic and geophysical data available, we choose this setting to highlight the capabilities of the inversion technique and to illustrate how it can incorporate surface as well as subsurface data. It is worth noting that even surface displacement away from the fault, such as GPS-derived coseismic displacements could be incorporated to find a more robust estimate of the remote stress tensor and the associated slip on the fault.

One of the limitations that is inherent to the proposed method is that knowledge of the unexposed geometry of the fault is required. However, in many settings ample information exists on the increasingly accurate relocations of seismicity, providing important insight into the structure and geometry of the fault of interest (e.g. Carena and Suppe, 2002). In the present case, we use subsurface geometries that fit the observed surface coseismic displacements

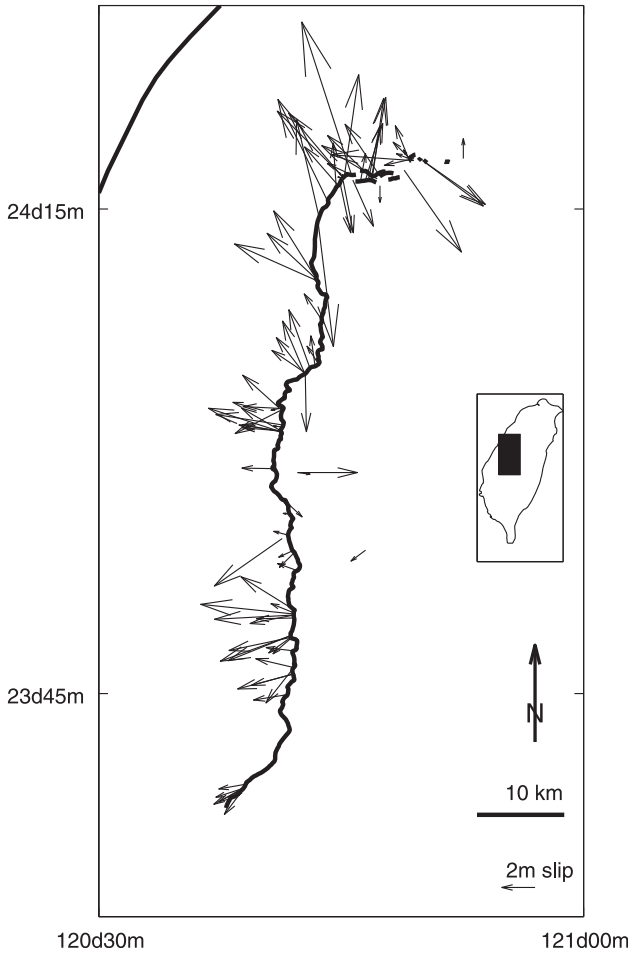


**Fig. 9.** Surface slip data of the 1999 Chi-Chi earthquake adapted from Blenkinsop (2006); fault traces of the Chelungpu fault are depicted in thick line; horizontal component of slip and slip magnitude plotted with arrows.

best, and combine these with the well documented geometry of the fault trace. Johnson and Segall (2004) fit a main fault dipping to the east at 26° to a depth of 12 km, a secondary fault segment dipping south at 23°, which joins the main fault by a third segment dipping shallowly to the southeast, and a horizontal décollement. Lee et al. (2002) attempt to fit a more refined geometry at depth that smoothly joins the separate sections and invert for slip on the resultant fault. Both studies find that maximum slip occurred in the northern section, near a bend in the surface trace (Lee et al., 2002). We incorporate the detailed surface trace, and the subsurface geometry by progressively smoothing the surface trace and projecting it at the preferred dip of 26° to a depth of 12 km. We omit the horizontal décollement to simplify the analysis. We further simplify the surface trace geometry at the northern end to represent the change in strike without incorporating all the different fault strands, but rather construct the fault to be one contiguous surface.

As input we use the surface slip data published by several workers (Lee et al., 2003; Blenkinsop, 2006), resolve these on the nearest elements at the surface and enforce that the recorded local strike of the fault trace is equal to the strike of the corresponding element. We average the slip measurements at locations with more than one offset markers recorded, while at others the triangular surface elements are large enough to necessitate that local slip measurements be averaged and resolved onto the respective elements. The resolved slip measurements are then imposed as

known boundary conditions in the inversion. We also include subsurface focal mechanism measurements relocated and inverted for by Wu et al. (2008), use the predicted rake, and scale the slip by the magnitude of each individual event in one of the inversions to highlight the capabilities of the algorithm. The material properties of the medium surrounding the fault are homogeneous, isotropic, and linearly elastic with a Poisson's ratio of 0.25 and a Young's modulus of 5 GPa. Because the lithologies across Taiwan are highly variable the values chosen should be understood as approximations to the effective material properties.

The inversion results highlight how the detailed surface slip data can produce robust remote stress orientations, while also providing an alternative method to estimating subsurface slip. The first inverse model only uses surface data and is depicted in Fig. 10b. Slip maxima occur at several locations with the largest near the bend in fault geometry at 24.2° latitude. The maximum slip is roughly 14m, which overestimates the 10m of slip in the subsurface from kinematic inversions using surface displacements records (Johnson and Segall, 2004; Lee et al., 2002). The direction of the most compressive principal stress (092.4°) indicates compression near the east-west direction and the stress ratio is $\phi = 0.169$. This result is close to that of faultless inversions (orientation of $\sigma_1 = 111°$, $\phi = 0.2$) considering the variance of stress orientation inversion results is 21°, which indicate in general that the principal stress direction, or orientation of crustal shortening, is roughly west–northwest to east–southeast (Blenkinsop, 2006). The deviation of regional principal stress orientations is likely due to averaging the slip data and simplifying the geometry near the northern end of the fault.

The second inverse model includes two focal mechanisms from the catalog of Wu et al. (2008) that occurred on the day of the main

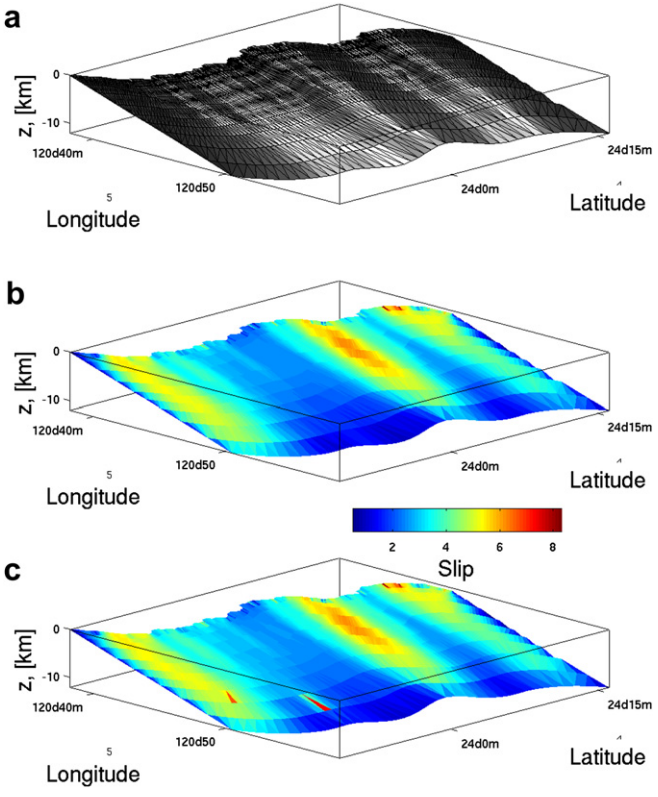


**Fig. 10.** a) The Chelungpu fault and the corresponding fault surface mesh used in the inversion. For slip vectors see Fig. 9 and Blenkinsop (2006). b) Slip distribution from the inversion using only the surface data. c) Slip distribution from the inversion using the surface slip data and the subsurface focal mechanism solutions.

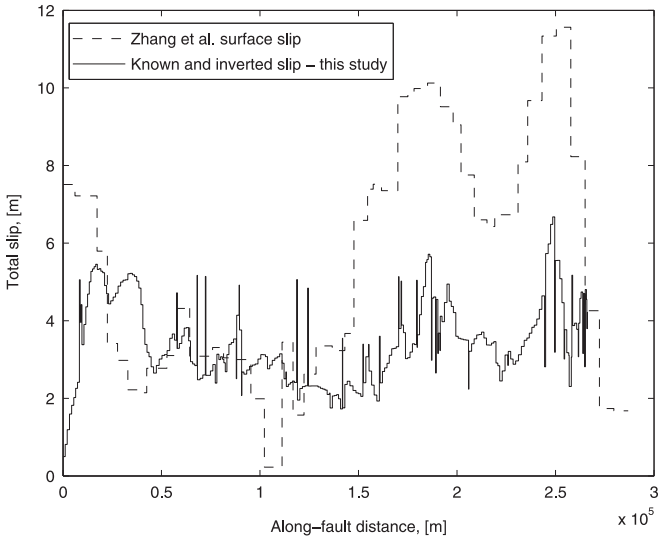


**Fig. 11.** Surface slip derived from Zhang et al. (2008) slip model (dashed line) and the slip model consisting of measured, resolved slip and slip solved for (solid line). Note that slip maxima in our model are lower as several surface slip measurements are averaged and resolved onto the fault geometry. Along fault length starts at the south-western end of the trace and continues to the north-eastern termination of the fault trace.

shock and are resolved onto the fault (Fig. 10c). The resultant slip on the fault is very similar to that of the inversion given above using only the surface data (Fig. 10b). One notable difference is the slight deviation of slip near the resolved focal mechanisms, which are enforced exactly. The most compressive principal stress orientation is 092.4° and the stress ratio is $\phi = 0.169$, identical to those using only the surface data (Fig. 10b).

The resultant surface slip comprised of the slip measurements resolved onto the fault geometry and resultant slip distribution we solved for reveals the high variability in surface slip with three broad areas of greater surface slip (centered on 25 km, 180 km, and 240 km along the fault trace) with intervening regions of lesser slip (Fig. 11). Slip maxima are generally lower than those reported at distinct points as the measurements are resolved onto the nearest fault element and when more than one measurement exists are averaged on the nearest fault element. The slip model derived from GPS and InSAR surface displacements by Zhang et al. (2008) reveals greater surface slip, but also exhibits three broad regions of high slip. While these two methods use much different data, they provide slip distributions with major similarities.

## 4. Conclusions

Faultless stress inversion methods are based on two assumptions that require careful evaluation when these methods are applied. In addition, their successful implementation requires diverse orientations of fault. The implications of ignoring this requirement have received little attention. We present a new stress inversion method that solves a complete mechanics problem explicitly including the stress perturbations of the faults. The complete mechanics problem requires knowledge of the fault geometry and some slip data, i.e. dip-slip or strike-slip component along portions of the fault, for the stress inversion and yields the remote stress tensor and the complete slip distribution, i.e. dip- and strike-slip component, along the entire fault.

We validate the method by solving a forward problem on two heuristic models and invert for stress and slip distributions using a subset of the elements in the forward problem. One heuristic model is that of a single fault with surface roughness similar to

faults encountered in the field at the outcrop ($\approx$10 m) scale (Sagy et al., 2007). The second heuristic model tests an array of circular faults with varying ranges in orientations. Principal stress orientation is reproduced to within a few degrees, often less. Principal stress magnitude ratios are reproduced well for the heuristic model of an array of faults with varying orientation, but rather poorly for the single fault heuristic model.

When compared to commonly used faultless methods, the proposed method performs as well for the heuristic model of a single rough fault for the principal stress orientations, but better for the ratio of principal stress magnitudes. For the heuristic model of an array of faults with varying orientations, the proposed method performs better in predicting the stress orientations and principal stress magnitudes.

Inversions for stress and slip distributions simultaneously for the 1999 Chi-Chi, Taiwan, earthquake provides robust results that compare well with principal stress orientations and ratios found in previous studies. The results here also compare well with slip distributions found using independent methods. Both inversion setups, one using only surface data, the other incorporating subsurface focal mechanisms as well, yield meaningful stress orientations and slip distributions. This application highlights the versatility of the proposed method.

## Acknowledgments

Financial support for this project was provided by the Stanford Rock Fracture Project. We appreciate thorough reviews by R.J. Lisle and an anonymous reviewer that improved the manuscript. Careful reviews by and interesting discussions with Paul Segall helped improve the manuscript. Thanks to the Igeoss consortium members for supporting the development of Poly3D. We thank Kaj Johnson for providing the coordinates of the Chelungpu fault trace. We also thank Lei Zhang for providing the results of his slip inversion.

## References

Aki, K., Richards, P., 2002. Quantitative Seismology. University Science Books, Sausalito, CA.
Amadei, B., Stephansson, O., 1997. Rock Stress and Its Measurement. Chapman & Hall, London.
Anderson, A., 1942. The Dynamics of Faulting and Dyke Formation with Application to Britain. Oliver and Boyd, Edinburgh.
Anderson, E.M., 1905. The dynamics of faulting. Edinburgh Geological Society Transactions. 8 (3), 387–402.
Anderson, T., 1995. Fracture Mechanics, Fundamentals and Applications. CRC Press, London, UK.
Angelier, J., 1984. Tectonic analysis of fault slip data sets. Journal of Geophysical Research 89, 5835–5848.
Angelier, J., Mechler, P., 1977. Sur une méthode graphique de recherche des contraintes principales également utiliable en tectonique et en séismologie: la méthode des dièdres driots. Bulletin de la Societé Géologique de France 7, 1309–1318.
Angelier, J., Tarantola, A., Valette, B., Manoussis, S., 1982. Inversion of field data in fault tectonics to obtain the regional stress - I. Single phase fault populations: a new method of computing the stress tensor. Geophysical Journal of the Royal Astronomical Society. 69, 607–621.
Armijo, R., Carey, E., Cisternas, A., 1982. The inverse problem in microtectonics and the separation of tectonic phases. Tectonophysics 82 (1–2), 145–160.
Aster, R., Borchers, B., Thurber, C., 2005. Parameter Estimation and Inverse Problems. Elsevier Academic Press, Burlington, MA, USA.
Atkinson, B., 1987. Fracture Mechanics of Rock. Academic Press, London, UK.
Aydin, A., Reches, Z., 1982. Number and orientation of fault sets in the field and in experiments. Geology 10, 107–112.
Blenkinsop, T., 2006. Kinematic and dynamic fault slip analyses: implications from the surface rupture of the 1999 Chi-Chi, Taiwan, earthquake. Journal of Structural Geology 28 (6), 1040–1050.
Blenkinsop, T., Lisle, R., Ferrill, D., 2006. Introduction to the special issue on new dynamics in palaeostress analysis. Journal of Structural Geology 28 (6), 941–942 (New dynamics in palaeostress analysis).
Bott, M., 1959. The mechanics of oblique slip faulting. Geological Magazine 96, 109–117.
Brune, J., 1968. Seismic moment, seismicity, and rate of slip along major fault zones. Journal of Geophysical Research 73, 777–784.
Bürgmann, R., Pollard, D., Martel, S., 1994. Slip distributions on faults: effects of stress gradients, inelastic deformation, heterogeneous host-rock stiffness, and fault interaction. Journal of Structural Geology 16, 1675–1688.
Carena, S., Suppe, J., 2002. 3D imaging of active structures using earthquake aftershocks: the Northridge thrust. Journal of Structural Geology 24, 887–904.
Carey, E., Brunier, B., 1974. Analyse thé orique et numérique d'un modélé mecanique élémentaire appliqué à l'étude d'une population de failles. Comptes Rendus hebdomadaires des seances de L'Academie des Sciences, Paris 279, 891–894.
Carey-Gailhardis, E., Mercier, J.L., 1987. A numerical method for determining the state of stress using focal mechanisms of earthquake populations: application to Tibetan teleseisms and microseismicity of southern Peru. Earth and Planetary Science Letters. 82, 165–179.
Choi, P. (1996). Reconstitutions des Paléocontraintes en Tectonique Cassante: Méthodes et Application aux Domaines Continentaux Déformés (Corée, Jura). PhD thesis, Université P. & M. Curie, Paris. 257 p.
Cladouhos, T.T., Allmendinger, R.W., 1993. Finite strain and rotation from fault-slip data. Journal of Structural Geology 15 (6), 771–784.
Comninou, M., Dunders, J., 1975. The angular dislocation in a half space. Journal of Elasticity 5, 205–216.
Couples, G., 1977. Stress and shear fracture (fault) patterns resulting from a suite of complicated boundary conditions with applications to the Wind River Mountains. Pure and Applied Geophysics 115, 113–133.
Crouch, S., Starfield, A., 1983. Boundary Element Methods in Solid Mechanics. George Allen and Unwin, London.
Dupin, J.-M., Sassi, W., Angelier, J., 1993. Homogeneous stress hypothesis and actual fault slip: a distinct element analysis. Journal of Structural Geology 15 (8), 1033–1043.
Etchecopar, A., Vasseur, G., Daignieres, M., 1981. An inverse problem in microtectonics for the determination of stress tensors from fault striation analysis. Journal of Structural Geology 3 (1), 51–65.
Fletcher, R., Pollard, D., 1990. Can we understand structural and tectonic processes and their products without appeal to a complete mechanics? Journal of Structural Geology 21, 1071–1088.
Fry, N., 1999. Striated faults: visual appreciation of their constraint on possible paleostress tensors. Journal of Structural Geology 21 (1), 7–21.
Fung, Y., 1977. A First Course in Continuum Mechanics. Prentice-Hall, Englewood Cliffs, NJ.
Gapais, D., Cobbold, P., Bourgeois, O., Rouby, D., deUrreistiete, M., 2000. Tectonic significance of fault-slip data. Journal of Structural Geology 22 (7), 881–888.
Gauthier, B., Angelier, J., 1985. Fault tectonics and deformation: a method of quantification using field data. Earth and Planetary Science Letters 74 (1), 137–148.
Gephart, J.W., 1990. FMSI: a fortran program for inverting fault/slickenside and earthquake focal mechanism data to obtain the regional stress tensor. Computational Geosciences. 16 (7), 953–989.
Gephart, J.W., Forsyth, D., 1990. An improved method for determining the regional stress tensor using earthquake focal mechanism data: application to the San Fernando earthquake sequence. Computational Geosciences. 16 (7), 953–989.
Griffith, A., 1921. The phenomena of rupture and flow in solids. Philosophical Transactions of the Royal Society A221, 163–198.
Griffith, A., 1925. Theory of rupture. In: Proceedings of the First International Congress for Applied Mechanics. Waltham Int. Press, Delft, pp. 53–64.
Hafner, W., 1951. Stress distribution and faulting. Geological Society of America Bulletin. 62, 373–398.
Hardcastle, K.C., Hills, L.S., 1991. Brute3 and select: Quickbasic 4 programs for determination of stress tensor configurations and separation of heterogeneous populations of fault-slip data. Computers & Geosciences 17 (1), 23–43.
Huang, Q., 1988. Computer-based method to separate heterogeneous sets of fault-slip data into sub-sets. Journal of Structural Geology 10 (3), 297–299.
Inglis, C., 1913. Stresses in a plate due to the presence of cracks and sharp corners. Transactions of the Institution of Naval Architects. 55, 219–230.
Irwin, G., 1957. Analysis of stresses and strain near the end of a crack traversing a plate. Journal of Applied Mechanics 24, 361–364.
Jackson, J., McKenzie, D., 1988. The relationship between plate motions and seismic moment tensors, and the rates of active deformation in the mediterranean and middle east. Geophysical Journal 93 (88), 46–73.
Jaeger, J., Cook, N., Zimmermann, R., 2007. Fundamentals of Rock Mechanics. Blackwell Publ., Malden, MA.
Jeyakumaran, M., Rudnicki, J., Keer, L., 1992. Modeling slip zones with triangular dislocation elements. Seismological Society of America Bulletin 82, 2153–2169.
Johnson, K., Segall, P., 2004. Imaging the ramp-décollement geometry of the chelungpu fault using coseismic GPS displacements from the 1999 Chi-Chi, Taiwan earthquake. Tectonophysics 378, 129–139.
Jones, L., 1988. Focal mechanisms and the state of stress on the San Andreas fault in southern California. Journal of Geophysical Research 93, 8869–8891.
Julien, P., Cornet, F.H., 1987. Stress determination from aftershocks of the Campania-Lucania earthquake of November 23, 1980. Annales Geophysicae 5B (3), 289–300.
Kao, H., Angelier, J., 2001. Stress tensor inversion for the Chi-Chi earthquake sequence and its implications on regional collision. Bulletin of the Seismological Society of America 91 (5), 1028–1040.
Kostrov, V., 1968. Seismic moment and energy of earthquakes, and seismic flow of rocks. Izvestiya Academy of Sciences of the USSR (Physics of Solid Earth) 1, 23–40.

Lawn, B., Wilshaw, T., 1993. Fracture of Brittle Solids. Cambridge University Press, New York.
Lay, T., Wallace, T., 1995. Modern Global Seismology. Academic Press, London, UK.
Lee, J.-C., Chu, H.-T., Angelier, J., Chan, Y.-C., Hu, J.-C., Lu, C., Rau, R.-J., 2002. Geometry and structure of northern surface ruptures of the 1999 Mw = 7.6 Chi-Chi Taiwan earthquake: influence from inherited fold belt structures. Journal of Structural Geology 24, 173–192.
Lee, Y.-H., Hsieh, M.-L., Lu, S.-D., Shih, T.-S., Wu, W.-Y., Sugiyama, Y., Azuma, T., Kariya, Y., 2003. Slip vectors of the surface rupture of the 1999 chi-chi earthquake, western taiwan. Journal of Structural Geology 25 (11), 1917–1931.
Liesa, C.L., Lisle, R.J., 2004. Reliability of methods to separate stress tensors from heterogeneous fault-slip data. Journal of Structural Geology 26 (3), 559–572.
Lisle, R.J., Orife, T.O., Arlegui, L., Liesa, C., Srivastava, D.C., 2006. Favoured states of palaeostress in the earth's crust: evidence from fault-slip data. Journal of Structural Geology 28 (6), 1051–1066 (New dynamics in palaeostress analysis).
Maerten, F., Maerten, L., Cooke, M., 2010. Solving 3D boundary element problems using constrained iterative approach. Computational Geosciences 14 (4), 551–564.
Maerten, F., Resor, P.G., Pollard, D.D., Maerten, L., 2005. Inverting for slip on three-dimensional fault surfaces using angular dislocations. Bulletin of the Seismological Society of America 95, 1654–1665.
Maerten, L., 2000. Variations in slip of intersecting faults: implications for paleostress inversion. Journal of Geophysical Research 105, 25553–25565.
Maerten, L., Willemse, E., Pollard, D., Rawnsley, K., 1999. Slip distributions on intersecting normal faults. Journal of Structural Geology 21, 259–271.
Malvern, I., 1969. Introduction to the Mechanics of a Continuum Medium. Prentice-Hall.
Mandl, G., 1988. Mechanics of Tectonic Faulting. Models and Basic Concepts. Elsevier, Amsterdam.
Marrett, R., Allmendinger, R.W., 1990. Kinematic analysis of fault-slip data. Journal of Structural Geology 12 (8), 973–986.
Martel, S., Shacat, C., 2006. Mechanics and interpretations of fault slip. In: Abercrombie, R., DiToro, G., Kanamori, H., McGarr, A. (Eds.), Radiated Energy and the Physics of Earthquake Faulting. American Geophysical Union Monograph, vol. 170, pp. 207–216.
McKenzie, D.P., 1969. The relation between fault plane solutions for earthquakes and the directions of the principal stresses. Bulletin of the Seismological Society of America. 59, 591–601.
Michael, A., 1987. Use of focal mechanisms to determine stress: a control study. Journal of Geophysical Research 92 (B1), 357–368.
Molnar, P., 1983. Average regional strain due to slip on numerous faults of different orientations. Journal of Geophysical Research 88, 6430–6432.
Mutlu, O., Pollard, D., 2008. On the patterns of wing cracks along an outcrop scale flaw: a numerical modeling approach using complementarity. Journal of Geophysical Research 113.
Nádai, A., 1931. Plasticity. McGraw-Hill, Inc., New York.
Nemcok, M., Lisle, R.J., 1995. A stress inversion procedure for polyphase fault/slip data sets. Journal of Structural Geology 17 (10), 1445–1453.
Orife, T., Arlegui, L., Lisle, R.J., 2002. Dipslip: a quickbasic stress inversion program for analysing sets of faults without slip lineations. Computers & Geosciences 28 (6), 775–781.
Orife, T., Lisle, R.J., 2003. Numerical processing of palaeostress results. Journal of Structural Geology 25 (6), 949–957.
Pollard, D., Fletcher, R., 2005. Fundamentals of Structural Geology. Cambridge University Press, Cambridge, UK.
Pollard, D., Saltzer, S., Rubin, A., 1993. Stress inversion methods: are they based on faulty assumptions? Journal of Structural Geology 15, 1045–1054.
Pollard, D., Segall, P., 1987. Theoretical displacements and stresses near fractures in rock: with applications to faults, joints, veins, dikes and solution surfaces. In: Atkinson, B. (Ed.), Fracture Mechanics of Rocks. Academic, San Diego.
Power, W., Tullis, T., Brown, S., Boitnott, G., Scholz, C., 1987. Roughness of natural fault surfaces. Geophysical Research Letters 14, 29–32.
Price, N.J., 1966. Fault and Joint Development in Brittle and Semi-brittle Rock. Pergamon, London.
Ramsay, J., Lisle, R., 2000. The Techniques of Modern Structural Geology. In: Applications of Continuum Mechanics in Structural Geology, vol. 3. Academic Press, London, UK.
Reches, Z., 1978. Number and orientation of fault sets in the field and in experiments. Tectonophysics 47, 109–129.
Reches, Z., 1987. Determination of the tectonic stress tensor from slip along faults that obey the coulomb yield condition. Tectonics 6 (4), 849–861.
Reinecker, J., Heidbach, O., Müller, B., Tingay, M., Connolly, P., 2004. The 2004 Release of the World Stress Map. http://www.world-stress-map.org.
Rice, J., 1980. The mechanics of earthquake rupture. In: Dziewonski, A., Boschi, E. (Eds.), Physics of the Earth's Interior, Proc. International School of Physics 'Enrico Fermi', Course 78, 1979. Italian Physical Society, North-Holland Publ. Co, pp. 555–649.
Roberts, G., Ganas, A., 2000. Fault-slip direction in central and southern Greece measured from striated and corrugated fault planes: comparison with focal mechanism and geodetic data. Journal of Geophysical Research 105 (B10), 23443–23462.
Rudnicki, J., 1980. Fracture mechanics applied to the Earth's crust. Annual Review of Earth and Planetary Sciences 8, 489–525.
Sagy, A., Brodsky, E., Axen, G., 2007. Evolution of fault-surface roughness with slip. Geology 35 (3), 283–286.
Sanford, A., 1959. Analytical and experimental study of simple geologic structures. Geological Society of America Bulletin. 70, 19–52.
Sato, K., Yamaji, A., 2006. Uniform distribution of points on a hypersphere for improving the resolution of stress tensor inversion. Journal of Structural Geology 28 (6), 972–979 (New dynamics in palaeostress analysis).
Segall, P., Pollard, D., 1980. Mechanics of discontinuous faults. Journal of Geophysical Research 85 4337–4350.
Shan, Y., Fry, N., 2005. A hierarchical cluster approach for forward separation of heterogeneous fault/slip data into subsets. Journal of Structural Geology 27 (5), 929–936.
Shan, Y., Li, Z., Lin, G., 2004. A stress inversion procedure for automated recognition of polyphase fault/slip data sets. Journal of Structural Geology 26 (9), 919–925.
Shan, Y., Lin, G., Li, Z., Zhao, C., 2006. Influence of measurement errors on stress estimated from single-phase fault/slip data. Journal of Structural Geology 28 (6), 943–951 (New dynamics in palaeostress analysis).
Shan, Y., Suen, H., Lin, G., 2003. Separation of polyphase fault/slip data: an objective-function algorithm based on hard division. Journal of Structural Geology 25 (6), 829–840.
Thomas, A. (1993). A Three-dimensional, Polygonal Element, Displacement Discontinuity Boundary Element Computer Program with Applications for Fractures, Faults, and Cavities in the Earth's crust. Master's Thesis, Stanford University, Stanford, California.
Twiss, R., Protzman, G., Hurst, S., 1991. Theory of slickenline patterns based on the velocity gradient tensor and microrotation. Tectonophysics 186, 215–239.
Twiss, R., Souter, B., Unruh, J., 1993. The effect of block rotations on the global seismic moment tensor and patterns of seismic p and t axes. Journal of Geophysical Research 98, 645–674.
Twiss, R., Unruh, J., 1998. Analysis of fault slip inversions: do they constrain stress or strain rate? Journal of Geophysical Research 103 (B6), 12205–12222.
van Gent, H., Back, S., Urai, J.L., Kukla, P., 2010. Small-sclae faulting in the upper cretaceous of the Groningen block (The Netherlands): 3D seismic interpretation, fault plane analysis and regional paleostress. Journal of Structural Geology 32, 537–553.
Vasseur, G., Etchecopar, A., Philip, H., 1983. Stress state inferred from multiple focal mechanisms. Annales Geophysicae. 1 (4–5), 291–298.
Voight, B., 1966. Beziehung zwischen großen horizontalen Spannungen in Gebirge und der Tektonik und der Abtragung. In: Proc. 1st Congr.. Int. Soc. Rock Mech., vol. 2, pp. 1–56. Lisbon.
Wallace, R., 1951. Geometry of shearing stress and relation to faulting. Journal of Geology 59, 118–130.
Whitcomb, J., Garmany, J., Anderson, D., 1974. Earthquake prediction: variation of seismic velocities before the San Fernando earthquake. Science 180, 632–635.
Willemse, E., 1997. Segmented normal faults: correspondence between three-dimensional mechanical models and field data. Journal of Geophysical Research 102 (B1), 675–692.
Willemse, E., Peacock, D., Aydin, A., 1997. Nucleation and growth of strike-slip faults in limestone from Somerset, UK. Journal of Structural Geology 12, 1461–1477.
Willemse, E., Pollard, D., Aydin, A., 1996. 3D analyses of slip distributions on normal fault arrays with consequences for fault scaling. Journal of Structural Geology 18, 1295–1309.
Williams, J., 1987. On the calculation of energy release rates for cracked laminates. International Journal of Fracture 36 (2), 101–119.
Wojtal, S., 1989. Measuring displacement gradients and strains in faulted rocks. Journal of Structural Geology 11 (6), 669–678.
Wu, Y.-M., Zhao, L., Chang, C.-H., Hsu, Y.-J., 2008. Focal mechanism determination in Taiwan by genetic algorithm. Bulletin of the Seismological Society of America 98 (2), 651–661.
Yamaji, A., 2000. The multiple inverse method: a new technique to separate stresses from heterogeneous fault-slip data. Journal of Structural Geology 22 (4), 441–452.
Yoffe, E.H., 1960. The angular dislocation. Philosophical Magazine. 5, 161–175.
Zhang, L., Wu, J.C., Ge, L.L., Ding, X.L., Chen, Y.L., 2008. Determining fault slip distribution of the Chi-Chi Taiwan earthquake with GPS and InSAR data using triangular dislocation elements. Journal of Geodynamics 45, 163–168.
Zoback, M., Zoback, M., Mount, V., etal, 1987. New evidence on the state of stress of the San Andreas fault system. Science 238, 1105–1111.
Zoback, M.L., 1992. First and second order patterns of stress in the lithosphere. The world stress map project. Journal of Geophysical Research 97, 11703–11728 (The World Stress Map Project).